ACOUSTIC HOLOGRAPHY WITH A CONCENTRIC RIGID AND OPEN SPHERICAL MICROPHONE ARRAY

Abhaya Parthy

School of Information Technologies
The University of Sydney, Australia
aparthy@it.usyd.edu.au

Craig Jin and André van Schaik

School of Electrical and Information Engineering
The University of Sydney, Australia
{craig,andre}@ee.usyd.edu.au

ABSTRACT

We present a new method and performance data related to volumetric acoustic intensity imaging using a spherical microphone array (SMA) consisting of a dual, concentric rigid and open SMA. The dual, concentric array was designed to improve the frequency range of a standard SMA. We apply standard techniques associated with interior spherical near-field acoustic holography (NAH) and, in particular, consider issues related to the optimal use of information from both arrays for NAH projection and the advantages that thus accrue from utilising a dual, concentric SMA.

***Index Terms*—** Array signal processing, Microphone arrays, Sound field recording, Spherical microphone array, Near-field acoustic holography

1. INTRODUCTION

Microphone array techniques associated with near-field acoustic holography (for review see [1]) and discrete inverse acoustic problems (for review see [2, 3]) have been well developed over the past several decades. Recently, there has been considerable development of interior spherical NAH using SMAs (see, e.g., [4–7]). SMAs present a wondrous opportunity to characterise, analyse, and recreate three-dimensional sound fields, which has probably led to the wealth of recent research. We have previously presented a dual, concentric rigid and open SMA comprised of 64 microphones, that is still compact, and which increases the available frequency range of analysis (see [8]). In this paper, we examine the consequences of employing a dual, concentric SMA for volumetric acoustic intensity imaging. That is to say, the holographic projection of the acoustic intensity field surrounding the SMA can be computed using a combination of interior NAH analysis applied to both the open and rigid arrays and we explore a method that combines information from both arrays in an optimal manner. We have not previously seen in the literature the application of this method of NAH analysis to a dual, concentric rigid and open SMA. We present real measurements and field data that demonstrate the performance capababilities.

2. METHODS

A dual, concentric rigid and open SMA was constructed by placing a rigid SMA at the center of a larger open SMA (see Figure 1). The rigid SMA was machined from a Nylon plastic, Ertalon, into two hemispherical halves resulting in a sphere with radius 1.63 cm. The open array was constructed using horizontal, circular steel rings mounted on a vertical steel ring, resulting in a sphere of radius 6.0 cm. Both spherical arrays were attached to and supported by a vertical, metallic rod. Thirty-two DPA type 4060-BM omnidirectional microphones were arranged on both the rigid and open spheres using a spherical 7-design optimised for discrete, spherical integration (described in [9]). The relative orientation of the rigid and open SMAs was left flexible. The microphone cables were neatly run along the support rod for the inner SMA and along the circular steel rings for the outer SMA. While it seems intuitively reasonable to distribute half of the sixty-four microphones to both SMAs in order to maximise the available frequency range, we have shown mathematically that this actually is the case (for details see [8]). In particular, we designed the dual, concentric SMA so that is has a minimum threshold signal-to-noise ratio of 30 dB when used as a constant third-order spherical harmonic beamformer over a 900 Hz to 16.0 kHz frequency range. The directivity of the system remains approximately constant across the frequency range by analyzing frequencies between 900 Hz and 2.84 kHz using the open SMA and frequencies between 2.84 kHz and 16 kHz with the rigid SMA (see [10]).

The performance of the dual, concentric SMA was analyzed by simultaneously measuring the acoustic tranfer functions for all 64 microphones for each of 393 directions around a sphere of radius 1 meter. The measurements were performed in an anechoic chamber with a loudspeaker mounted on a robotic arm that could rotate about the center of the chamber with a precision better than one degree of spherical angle. The acoustic transfer functions were measured using a log sine sweep (8 s, 100 Hz to 20 kHz). To make the recordings we used eight 8-channel Pro Tools Digidesign Pre preamplifiers with digital gain settings and four 16-channel Apogee AD-16X analogue-to-digital converters (48 kHz sample rate, 24-bit resolution). The ADAT output from the analogue-to-digital converters is sent to a RME ADI-648 MADI-to-ADAT converter, which converts the eight 8-channel ADAT signals to one 64-channel MADI signal. The 64 microphone signals, in MADI format, are recorded onto a personal computer (PC) using a RME Hammerfall DSP MADI PCI sound card. The PC is a standard workstation computer with an Intel Core 2 Duo CPU running at 2.4 GHz and with 2 GB of RAM.

2.1. NAH using a dual, concentric SMA

The primary issue addressed in this paper is how to use a dual SMA appropriately for volumetric imaging using NAH. In other words, with the dual, concentric SMA there are two measurement surfaces and one would like to combine information optimally and robustly. As the spherical coordinate system is separable, NAH proceeds by first determining the holographic projection coefficients based on the Fourier-Bessel representation. The projection coefficients, $P_{mn}(k)$, are determined from the acoustic pressure measurements, $p(kr, \Omega_j)$

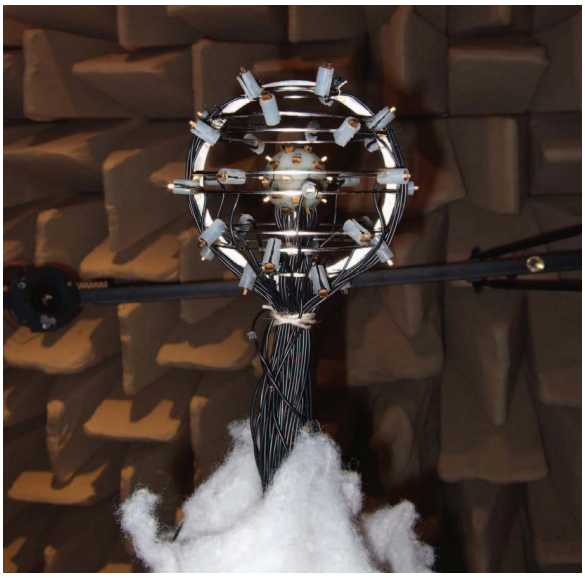

Fig. 1. A photo is showing the dual, concentric SMA located inside the anechoic chamber in which its' performance was measured. The moveable loudspeaker is shown to the left of the SMA.

as shown below:

$$P_{mn}(k) = \sum_{j=1}^{M} \alpha_j \frac{p(kr, \Omega_j)}{b_n(kr, ka)} Y_n^{m*}(\Omega_j), \quad (1)$$

where, $k = \frac{2\pi}{\lambda}$, is the wave number, λ, is the wavelength, r, is the radius at which the sound pressure is measured, $a \leq r$, is the radius of the inner rigid spherical baffler, $\Omega_j = (\theta_j, \phi_j)$, is the angular position of microphone j on the spherical microphone array in spherical coordinates, $M = 32$, is the number of microphones on either the open or rigid SMA, $\alpha_j = \frac{4\pi}{M}$, is a weight for each position related to the spatial sampling scheme, $p(kr, \Omega_j)$, is the pressure recorded by the microphone at position Ω_j on the spherical microphone array, $b_n(kr, ka)$ is a modal coefficient, and $Y_n^m(\cdot)$ are the spherical harmonic functions. The $Y_n^m(\cdot)$ are defined as

$$Y_n^m(\Omega) = Y_n^m(\theta, \phi) = \sqrt{\frac{2n+1}{4\pi} \frac{(n-m)!}{(n+m)!}} P_n^m(\cos\theta) e^{im\phi}, \quad (2)$$

where, $P_n^m(\cdot)$, is the associated Legendre function. Note that complex conjugation is denoted by an asterisk. For the dual, concentric SMA, $b_n(kr, ka)$, is defined as

$$b_n(kr, ka) = j_n(kr) - \frac{j_n'(ka)}{h_n'(ka)} h_n(kr), \quad (3)$$

where k, r and a are as defined previously, $j_n(\cdot)$, $j_n'(\cdot)$, $h_n(\cdot)$, and $h_n'(\cdot)$ are the spherical Bessel function, the spherical Hankel function of the second-kind, and their derivatives, respectively, and $i = \sqrt{-1}$.

Once the holographic projection coefficients are determined one can project or propagate the sound field to a new radius using the following equations:

$$P(k\hat{r}, \Omega_0) = \sum_{n=1}^{N} P_{mn}(k)\, j_n(k\hat{r}) \sum_{m=-n}^{n} Y_n^m(\Omega_0), \quad (4)$$

$$v_r(k\hat{r}, \Omega_0) = \sum_{n=1}^{N} P_{mn}(k) \frac{j_n'(k\hat{r})}{-i\rho c} \sum_{m=-n}^{n} Y_n^m(\Omega_0), \quad (5)$$

$$v_\theta(k\hat{r}, \Omega_0) = \sum_{n=1}^{N} P_{mn}(k) \frac{j_n(k\hat{r})}{-i\hat{r}^2 k\rho c} \sum_{m=-n}^{n} \frac{\partial Y_n^m(\Omega_0)}{\partial\theta}, \quad (6)$$

$$v_\phi(k\hat{r}, \Omega_0) = \sum_{n=1}^{N} P_{mn}(k) \frac{j_n(k\hat{r})}{-i\hat{r}^2 \sin^2(\theta) k\rho c} \sum_{m=-n}^{n} \frac{\partial Y_n^m(\Omega_0)}{\partial\phi}, \quad (7)$$

where $P(k\hat{r}, \Omega_0)$ is the pressure, $v_r(k\hat{r}, \Omega_0)$ is the radial velocity, $v_\theta(k\hat{r}, \Omega_0)$ is the velocity in the θ-direction, $v_\phi(k\hat{r}, \Omega_0)$ is the velocity in the ϕ-direction, $\hat{r}$ is the projection radius, Ω_0 is the projection angle in spherical coordinates, ρ is the density of air, c is the speed of sound, N is the truncation order for the Fourier-Bessel expansion and the other terms are as defined previously. Note that the above equations differ slightly from those given in [1] because we have expressed $v_\theta(k\hat{r}, \Omega_0)$ and $v_\phi(k\hat{r}, \Omega_0)$ in radians. The acoustic intensity field is given by $\frac{1}{2}\Re(P\bar{v}^*)$. The equation given for the calculation of the holographic projection coefficients, $P_{mn}(k)$, highlights the fact that the pressure measurements are scaled by the modal coefficients, $b_n(kr, ka)$. This scaling removes the dependence of the projection coefficients on the radius of the measurement surface. In other words, the $P_{mn}(k)$ should in some sense be independent of the measurement surface and, in particular, independent of whether the rigid or open measurement surface is used for their calculation. However, this is not actually the case with real measurements because the modal coefficients are different for the two measurement surfaces (see Figure 2). The physical implications of this difference are that for a given sound field the modal coefficients provide a measure of the signal level that is present at the microphones on the measurement surface for a given order of the Fourier-Bessel representation. Thus, we propose a simple and effective means for calculating the holographic projection coefficients: Use the projection coefficients which are associated with the measurement surface with the larger modal coefficient for a given order of the Fourier-Bessel expansion.

2.2. Regularisation, Spatial Aliasing, and Measurement Noise

The impact of spatial aliasing error, microphone placement error and measurement noise error on the performance of the dual, concentric SMA is similar for both beamforming and NAH. In designing the dual, concentric SMA we made extensive theoretical calculations of these errors (see [8]) to ensure that the array would operate at third-order for the specified frequency range (900 Hz to 16.0 kHz). The description of array errors differs slightly for beamforming [11] and NAH [7], but the mathematical essence is the same. Spatial aliasing error limits performance at the higher frequencies, while measurement noise error limits performance at the lower frequencies. Spatial aliasing error arises when the Fourier-Bessel expansion used for the holographic projection (refer to Eqn.'s 4–7) is truncated to a finite order (N). This truncation provides a method to regularise the holographic projection solution and is similar to the k-space filter commonly used in planar NAH (see [1] for details). In [11], Rafaely derives the spatial aliasing error and the measurement noise error for a SMA in a plane-wave soundfield with the array looking in the direction of the plane-wave, as is common in the literature. Using Rafaely's error formulation we demonstrate in [10] that our dual, concentric SMA is accurately described by these errors in practice as well as in theory.

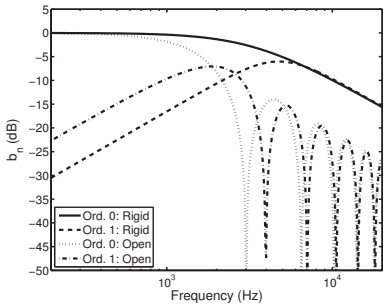

(a)

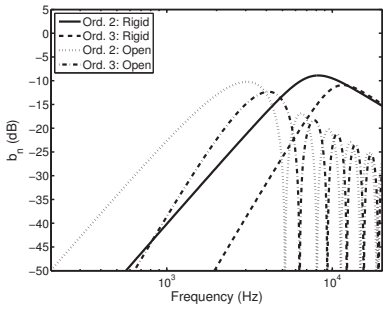

(b)

Fig. 2. The amplitude of the modal coefficient for the inner rigid SMA, and the outer open SMA is shown for, (a), orders zero and one and, (b), orders two and three.

3. RESULTS

In Figure 3 we show the acoustic intensity field that is obtained when NAH is naively applied to the dual, concentric SMA for a 2600 Hz sound source located on the x-axis at 1 m from the center of the array (as described in Section 2). By naively, we mean that we do not combine projection coefficients from the two SMAs. We show a holographic projection of the acoustic intensity field as projected outward from the inner rigid array to a 2 cm projection radius. We also show a holographic projection of the acoustic intensity field as projected inward from the outer array to a 5 cm projection radius. Note that all holographic projections described in this section are truncated to third order. For this first example, we have purposefully selected a frequency at the boundary of which either the rigid or open array can operate. What we would like to highlight is that even at these relatively small projection distances, we do not obtain a correct holographic projection. For example, the field projection using the open array clearly has too much curvature. We can start to correct and compensate for these defaults by selecting a combination of projection coefficients from the inner and outer arrays based on the modal coefficients as described in Section 2.1. So, for example, consider now Figures 4(a) and 4(b) which constrasts naive projection with "combination projection". In these figures, we show holographic projection of the acoustic intensity field at a projection radius of 3.13 cm (the geometric mean of the inner and outer array) for a 2850 Hz sound source located on the x-axis at 1 m. For the combination projection, the order-0 and order-1 projection coefficients are determined from the rigid array, while the order-2 and order-3 coefficients are determined from the open array (refer to Figure 2). Each figure actually shows two projections, one for the combination

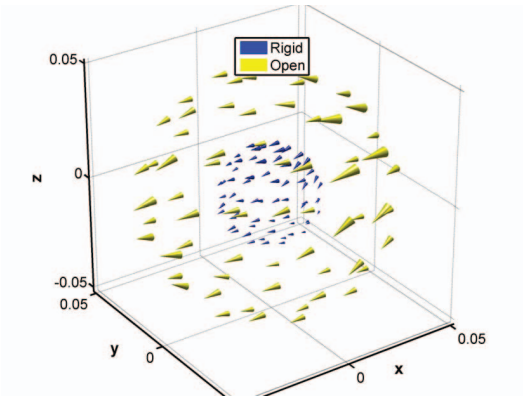

Fig. 3. Naive holographic projection is shown; details as in text.

projection and one for the naive projection. Clearly, the combination projection gives better performance and allows the array to operate in a region it would not normally be able to do so. Similarly, Figures 5(a) and 5(b) show a holographic projection at a projection radius of 2.0 cm for a 5000 Hz source located on the x-axis at 1 m. At this frequency for the combination projection, the order-0, order-1, and order-2 coefficients are determined from the rigid array and the order-3 coefficients are determined from the open array (refer to Figure 2). Again, we see a clear improvement in the quality of the holographic projection.

In order to quantify the above results, we used the rigid and open arrays to estimate the free-field sound pressure field (i.e., the pressure field without the array present and with no scattering from the rigid spherical baffle) at their corresponding measurement surfaces at the 32 microphone positions and treat this as ground truth. We then used the projection coefficients from the rigid array alone and the open array alone to estimate the pressure field at *both* measurement surfaces and compare this with the pressure estimates obtained at both measurement surfaces using the combination projection techniqe. The total relative error in the pressure estimations (i.e., the absolute value of the error in the pressure value divided by the pressure value) that were obtained for the 2850 Hz source and 5000 Hz source across both measurement surfaces are shown in Table 1. The combination projection technique again demonstrates a clear advantage.

Frequency	Rigid Array	Open Array	Combination
2800 Hz	86.30	184.01	15.58
5000 Hz	36.16	55.91	30.43

Table 1. The total relative error in free-field pressure estimation is shown. Details as in text.

4. CONCLUSION

In this paper, we present a novel method for NAH using a dual, concentric SMA. This method combines holographic projection coefficients from the open and rigid array based on the modal coefficients. Field measurements demonstrate that this technique improves the holographic projection of the acoustic intensity field. In future work, we will examine partial field decomposition techniques using a dual, concentric SMA (e.g., see [12]).

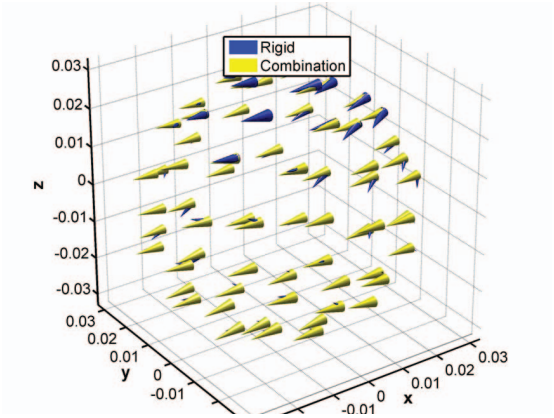

(a)

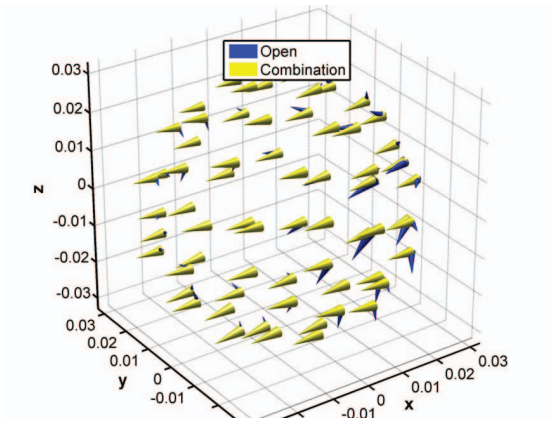

(b)

Fig. 4. Figure 4(a) contrasts combination projection with outward naive projection from the inner rigid array, and Figure 4(b) contrasts combination projection with inward naive projection from the outer open array (2850 Hz, 3.13 cm).

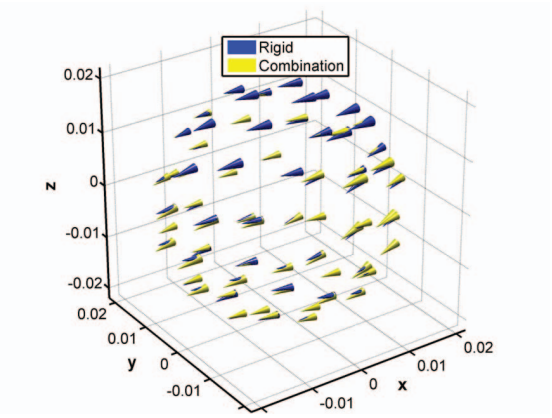

(a)

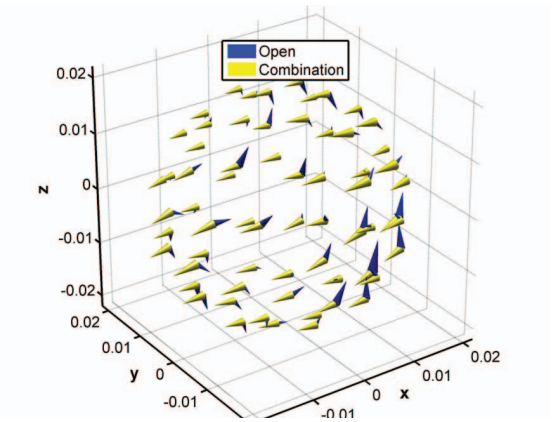

(b)

Fig. 5. Figure 5(a) contrasts combination projection with outward naive projection from the inner rigid array, and Figure 5(b) contrasts combination projection with inward naive projection from the outer open array (5000 Hz, 2.0 cm).

5. REFERENCES

[1] E. Williams, *Fourier Acoustics Sound Radiation and Nearfield Acoustical Holography*, Academic Press, Sydney, 1999.

[2] P. Nelson and S. Yoon, "Estimation of acoustic source strength by inverse methods: part I, conditioning of the inverse problem," *J. Sound and Vib.*, vol. 233, no. 4, pp. 639–664, 2000.

[3] S. Yoon and P. Nelson, "Estimation of acoustic source strength by inverse methods: part II, experimental investigation of methods for choosing regularization parameters," *J. Sound and Vib.*, vol. 233, no. 4, pp. 665–701, 2000.

[4] B. Rafaely, "Analysis of enclosed sound fields using spherical microphone array processing," *J. Acoust. Soc. Am.*, vol. 123, no. 5, pp. 3308, 2008.

[5] K. Haddad and J. Hald, "3d localization of acoustic sources with a spherical array," *J. Acoust. Soc. Am.*, vol. 123, no. 5, pp. 3311, 2008.

[6] E. Williams and K. Takashima, "Vector intensity reconstructions in a volume surrounding a rigid spherical measurement array," *J. Acoust. Soc. Am.*, vol. 123, no. 5, pp. 3309, 2008.

[7] E. Williams, N. Valdivia, P. Herdic, and J. Klos, "Volumetric acoustic vector intensity imager," *J. Acoust. Soc. Am.*, vol. 120, no. 4, pp. 1887–1897, 2006.

[8] A. Parthy, C. Jin, and A. van Schaik, "Optimisation of co-centred rigid and open spherical microphone arrays," in *120th AES Conv.*, Paris, France, 2006.

[9] R.H. Hardin and N.J.A. Sloane, "Mclaren's improved snub cube and other new spherical designs in three dimensions," *Discrete and Comp. Geom.*, vol. 15, no. 4, pp. 429–441, 1996.

[10] A. Parthy, C. Jin, and A. van Schaik, "Measured and theoretical performance comparison of a co-centred rigid and open spherical microphone array," in *Int. Conf. Audio, Language and Image Proc.*, July 2008, pp. 1289–1294.

[11] B. Rafaely, "Analysis and design of spherical microphone arrays," *IEEE Trans. on Speech and Audio Proc.*, vol. 13, no. 1, pp. 135–143, Jan. 2005.

[12] J. Hald, "STSF - a unique technique for scan-based near-field acoustic holography without restrictions on coherence," *Bruel and Kjaer Technical Review No. 1 - 1989*, 1989.